JGR Biogeosciences

RESEARCH ARTICLE
10.1029/2021JG006416

Drought-Induced Salinity Enhancement Weakens Mangrove Greenhouse Gas Cycling

Xudong Zhu[1,2], Chenyang Sun[1], and Zhangcai Qin[2,3]

[1]Key Laboratory of the Coastal and Wetland Ecosystems (Ministry of Education), State Key Laboratory of Marine Environment Science, Taiwan Strait Marine Ecosystem National Observation and Research Station, Coastal and Ocean Management Institute, College of the Environment and Ecology, Xiamen University, Xiamen, Fujian, China, [2]Southern Marine Science and Engineering Guangdong Laboratory (Zhuhai), Zhuhai, Guangdong, China, [3]Key Laboratory of Tropical Atmosphere-Ocean System (Ministry of Education), School of Atmospheric Sciences, Sun Yat-sen University, Zhuhai, Guangdong, China

Key Points:

- Eddy covariance measurements of ecosystem-level greenhouse gas (GHG) fluxes of CO_2 and CH_4 in a subtropical estuarine mangrove are presented
- The warming effect from CH_4 emissions can partially offset the cooling effect from mangrove CO_2 uptake
- Drought-induced salinity enhancement due to reduced rainfall and river discharge weakens mangrove GHG cycling

Correspondence to:
X. Zhu,
xdzhu@xmu.edu.cn

Citation:
Zhu, X., Sun, C., & Qin, Z. (2021). Drought-induced salinity enhancement weakens mangrove greenhouse gas cycling. *Journal of Geophysical Research: Biogeosciences*, *126*, e2021JG006416. https://doi.org/10.1029/2021JG006416

Received 23 APR 2021
Accepted 2 AUG 2021

Author Contributions:
Conceptualization: Xudong Zhu, Zhangcai Qin
Formal analysis: Xudong Zhu, Chenyang Sun, Zhangcai Qin
Funding acquisition: Xudong Zhu
Investigation: Xudong Zhu, Chenyang Sun
Methodology: Xudong Zhu, Chenyang Sun, Zhangcai Qin
Project Administration: Xudong Zhu
Supervision: Xudong Zhu
Validation: Xudong Zhu
Visualization: Xudong Zhu, Chenyang Sun
Writing – original draft: Xudong Zhu, Chenyang Sun
Writing – review & editing: Xudong Zhu, Zhangcai Qin

Abstract

The importance of tidal mangroves in mitigating greenhouse gas (GHG) *via* sequestering atmospheric carbon dioxide (CO_2) has been increasingly recognized, but this climate benefit comes at a biogeochemical cost of methane (CH_4) emissions. Previous studies have assessed the net radiative effect of mangrove GHG fluxes, however, large uncertainty still exists due to the very limited availability of long-term continuous measurements. In this study, we analyzed the temporal variations of GHG (CO_2 and CH_4) fluxes and their environmental controls based on eddy covariance measurements in a subtropical estuarine mangrove in the Southeast China during 2019 and 2020, when a severe drought occurred. The results showed (a) annually this mangrove acted as a CO_2 sink of −1,075.8 g C m^{-2} and a CH_4 source of 3.1 g C m^{-2}, and the CH_4-induced warming effect can offset 4.6% (9.8%) of the CO_2-induced cooling effect at a 100-year (20-year) time horizon using the metric of sustained-flux global warming potentials; (b) net CO_2 and CH_4 fluxes showed different diurnal and seasonal variation patterns, with stronger CO_2 sink and CH_4 source in colder and warmer seasons, respectively; (c) drought-induced salinity enhancement due to reduced rainfall and river discharge weakened GHG cycling, lowering both CO_2 sink and CH_4 source in the drier year. This study confirms that ecosystem-level CH_4 emissions from estuarine mangroves are not negligible and could substantially offset the CO_2-induced cooling effect. Future increases in temperature and salinity with expected global warming and sea level rise will likely weaken the climate benefits of mangroves.

Plain Language Summary

Tidal mangroves have a climate benefit via sequestering atmospheric carbon dioxide, but this benefit could be offset by their methane emissions. Due to the lack of long-term continuous and simultaneous measurements of these two greenhouse gas fluxes, we're short of the knowledge on the extent of this climate offset. Drought-induced salinity enhancement could suppress carbon dioxide and methane exchanges given the recognized role of salinity stress on mangrove biogeochemistry. Based on one-and-a-half-year flux tower measurements capturing a severe spring/summer drought event, we examine the responses of greenhouse gas fluxes to environmental factors in particular for drought in a subtropical estuarine mangrove in the Southeast China. As a carbon dioxide sink and a methane source, this mangrove sequesters more carbon dioxide in colder seasons but emits more methane in warmer seasons. Drought-induced salinity enhancement due to reduced rainfall and river discharge weakens greenhouse gas cycling, simultaneously lowering carbon dioxide sink and methane source. This study confirms that the warming effect from methane emissions could substantially offset the cooling effect from carbon dioxide uptake. Future climate change including higher temperature and salinity will likely weaken the climate benefits of mangroves.

1. Introduction

Tidal mangroves are one of the most important blue carbon ecosystems that have been increasingly recognized as effective long-term natural carbon sinks for climate change mitigation (Howard et al., 2017; Nellemann & Corcoran, 2009). As a carbon-rich and highly productive coastal ecosystem (Ouyang & Lee, 2020), mangrove forests can sequester atmospheric greenhouse gas (GHG) of CO_2 and capture suspended carbon during tidal inundation at much larger rates per unit area than inland forests (Alongi, 2014; Breithaupt

et al., 2012; McLeod et al., 2011). Despite of their small global extent (<0.1% of continental surface (Giri et al., 2011)), mangroves play a disproportionately large role in regional and global carbon cycling (McLeod et al., 2011). The world's mangroves are being alarmingly lost at an average annual rate of 0.16% between 2000 and 2012 (Hamilton & Casey, 2016). This deforestation reduces mangrove blue carbon by ~0.08 Pg C $year^{-1}$, accounting for 6% of the world's annual carbon emissions from land use and land cover change (Hamilton & Friess, 2018; Le Quéré et al., 2018). Therefore, the priority of protection and restoration of mangroves as blue carbon ecosystems has been widely called (McLeod et al., 2011; Murdiyarso et al., 2010; Sasmito et al., 2019).

Globally, the net primary productivity of mangroves is estimated to be ~200 Tg C $year^{-1}$ (Alongi, 2014), of which ~20% is returned back to the atmosphere *via* sediment respiratory efflux, ~60% is laterally exported *via* litters or particular/dissolved carbon, and the remaining (i.e., natural carbon sinks) is stored in vegetation biomass or buried in sediments (Alongi & Mukhopadhyay, 2014; Rosentreter et al., 2018a). During the process of carbon burial, methanogenic archaea produce another GHG of CH_4 in anoxic sediments (Al-Haj & Fulweiler, 2020; Bridgham et al., 2013), and consequent CH_4 emissions offset carbon sinks initially removed from the atmosphere. Despite the magnitude of CH_4 emissions is relatively small, only accounting for <10% of total carbon mineralization (Kristensen, 2007), the radiative forcing of CH_4, expressed as sustained-flux global warming potential (SGWP), is 45 (or 96) times of CO_2 over a 100-year (or 20-year) time horizon (Neubauer & Megonigal, 2015). Therefore, CH_4 emissions have the potential to weaken the contribution of mangrove blue carbon to climate change mitigation (Rosentreter et al., 2018b; Zheng et al., 2018). A recent global estimation of the CH_4 offset potential indicated that mangrove sediment and water CH_4 emissions offset 20% of blue carbon burial over a 20-year time horizon (Rosentreter et al., 2018b).

Mangroves are generally assumed to be weak CH_4 sources due to the presence of sulfate in mangrove sediments, in which anaerobic methanogenesis is outcompeted by sulfate reduction (Alongi, 2009; Kristensen, 2007). However, in comparison with mangrove CO_2 uptakes, the uncertainty in mangrove CH_4 emissions is much larger, varying from −0.8 to 874.4 mg CH_4-C m^{-2} day^{-1} (Al-Haj & Fulweiler, 2020). This large uncertainty limits the ability to accurately quantify the potential of CH_4 emissions to offset mangrove blue carbon. In addition to physical inaccessibility of harsh mangrove habitats, the uncertainty is mainly caused by diversified habitats with contrasting hydroperiod/salinity settings, strong temporal and spatial heterogeneity of GHG fluxes, and imperfect sampling/measuring techniques. First, according to hydrological influence, mangrove habitats can be classified into three types including estuarine/riverine, fringe, and basin/interior mangroves (Ewel et al., 1998), which experience contrasting hydroperiod and salinity gradients. Among these three habitats, estuarine mangroves are likely the strongest CH_4 emitter with lower salinity from more freshwater inputs and higher nutrient concentrations from heavier anthropogenic activities (Zheng et al., 2018). Second, mangrove CH_4 emissions are mainly determined by CH_4 production below water table, oxidation above water table, and transport processes (diffusion, ebullition, and plant-mediated paths) (Bridgham et al., 2013). These processes are temporally varying and/or spatially heterogeneous since they are regulated by a variety of biotic and abiotic factors including mangrove species/sediment compositions, hydroperiod/salinity regimes, and meteorological conditions. For estuarine mangroves, CH_4 emissions might be more regulated by variable freshwater-saltwater inputs, and thus temporal variations in rainfall, river discharge, and tidal activities could significantly change the magnitudes of salinity/sulfate and CH_4 emissions (Cabezas et al., 2018; Welti et al., 2017). Third, most of mangrove GHG flux studies are based on chamber-based gas flux techniques, which suffer from several issues such as chamber disturbances on in-situ temperature/light conditions, logistical inability to conduct continuous measurements with periodical tidal inundation, and spatial/temporal misrepresentation of measured fluxes. On the one hand, mangrove GHG fluxes are diurnally and seasonally variable (Alongi, 2014) and thus temporally discontinuous chamber-based measurements could lead to large bias in GHG budgets. On the other hand, the significance of plant-mediated CH_4 transport paths including stems (Jeffrey et al., 2019), canopies (Keppler et al., 2006), and pneumatophores (Kreuzwieser et al., 2003) has been identified and thus chamber-based measurements without covering plant-mediated emissions could underestimate total mangrove CH_4 emissions.

The EC technique has been widely used in various ecosystems to measure GHG fluxes over the past two decades (Baldocchi et al., 2001; Baldocchi, 2019), with recently increasing EC applications in mangroves (Alvarado- Barrientos et al., 2020; Barr et al., 2010; Chen et al., 2014; Cui et al., 2018; Leopold et al., 2016;

Liu & Lai, 2019; Rodda et al., 2016). These EC studies provide long-term continuous ecosystem fluxes with improved spatial/temporal representations, but few of them simultaneously measure CO_2 and CH_4 fluxes in mangroves (Knox et al., 2019), which strongly limits the ability to accurately quantify the magnitudes of GHG fluxes and their contributions to net GHG balance. Based on 3-year continuous EC measurements in a subtropical estuarine mangrove, Liu et al. (2020) found that ecosystem CH_4 emissions could offset half of the radiative cooling effect by CO_2 uptakes over a 20-year time horizon, highlighting the critical role of CH_4 emissions in regulating net GHG balance. However, more EC-based GHG flux measurements are highly needed to assess whether this strong CH_4 offset potential is applicable to other estuarine mangroves.

In this study, we analyze 1.5-year EC measurements of simultaneous CO_2 and CH_4 fluxes in a subtropical estuarine mangrove of Southeast China between August 2019 and December 2020, when a severe drought occurred with reduced rainfall than the multi-year average. Less freshwater inputs from reduced rainfall and river discharge will increase the salinity level in estuarine mangroves, which could suppress both ecosystem CO_2 and CH_4 fluxes given the recognized role of salinity stress on plant/sediment biogeochemistry in mangroves (Lee et al., 2008; Robertson & Alongi, 2016; Takemura et al., 2000). The objectives of this study are to: (a) examine diurnal and seasonal variations in GHG fluxes (CO_2 and CH_4), (b) quantify each GHG budget and their net radiative forcing, and (c) assess environmental controls on GHG fluxes with more focus on the salinity effect on GHG cycling. We hypothesize: (a) ecosystem CH_4 emissions from this low-salinity mangrove wetland are not negligible and will partially offset the radiative cooling effect from ecosystem CO_2 uptakes, and (b) drought-induced salinity enhancement will weaken mangrove GHG cycling.

2. Materials and Methods

2.1. Study Site

The study site, Yunxiao mangrove flux tower (23.9240°N, 117.4147°E) of ChinaFLUX and USCCC networks, is located in a subtropical estuarine wetland to the south of Zhangjiang river running into Taiwan Strait (~30 km away) of Southeast China (Figure 1). This wetland experiences a semidiurnal tidal cycle with mean tidal range of ~2 m, and a prevalent northwest-southeast wind direction. It has a monsoon climate with mean annual air temperature of ~21°C and mean annual rainfall of ~1,715 mm. Distinct dry (October – March) and wet (April – September) seasons can be identified. The mangrove forests around the flux tower are mainly comprised of *Kandelia obovata*, *Avicennia marina*, and *Aegiceras corniculatum*, and the understory sediment surface is usually inundated twice a day (up to ~1 m tidal height). See Lin (2001); Zhu, Hou, et al. (2019); Zhu, Hou, et al. (2021) and Zhu, Qin, et al. (2021) for more details on the study site. All permits on research activities in this site were acquired from the Zhangjiang Estuary Mangrove National Nature Reserve Administration.

2.2. GHG Flux and Ancillary Measurements

The GHG fluxes between mangrove and the atmosphere at a temporal interval of 30-min, including net ecosystem CO_2 exchange (NEE) and net ecosystem CH_4 exchange (NME), were calculated from raw 10-Hz measurements from an EC system (Figure 1a) mounted on a mangrove flux tower (Figure 1b). The EC system consisted of a three-axis sonic anemometer (CSAT-3, Campbell Scientific, Inc., Logan, UT, USA) and two open-path gas analyzers of CO_2 and CH_4 (LI-7500 and LI-7700, Li-COR Inc., Lincoln, NE, USA). All these sensors were mounted ~2 m above the canopy on the flux tower, and more than 90% of the fluxes originated from mangrove forests within 100 m around the tower. Ancillary 30-min meteorological data used in this study included air temperature (HMP155A sensor, Vaisala, Helsinki, Finland), 10-cm soil temperature (soil thermocouple probe, model 109, Campbell Scientific, Inc.), rainfall (TE525MM Rain Gage, Campbell Scientific, Inc.), photosynthetically active radiation (PAR; PQS1 PAR Quantum sensor, Kipp & Zonen, Delft, Netherlands), vapor pressure deficit (VPD; derived from measured air temperature and relative humidity by HMP155A sensor, Vaisala). Ancillary 30-min tidal data used in this study included surface water salinity and surface water level. Surface water salinity was estimated from measured electronic conductivity and water temperature by HOBO U24-002-C Conductivity Logger (Onset, Bourne, MA, USA), using the Practical Salinity Scale 1978 equations (Lewis & Perkin, 1981). Surface water level was estimated from measured pressure difference between one pressure sensor (HOBO U20L-04 Water Level Logger, Onset)

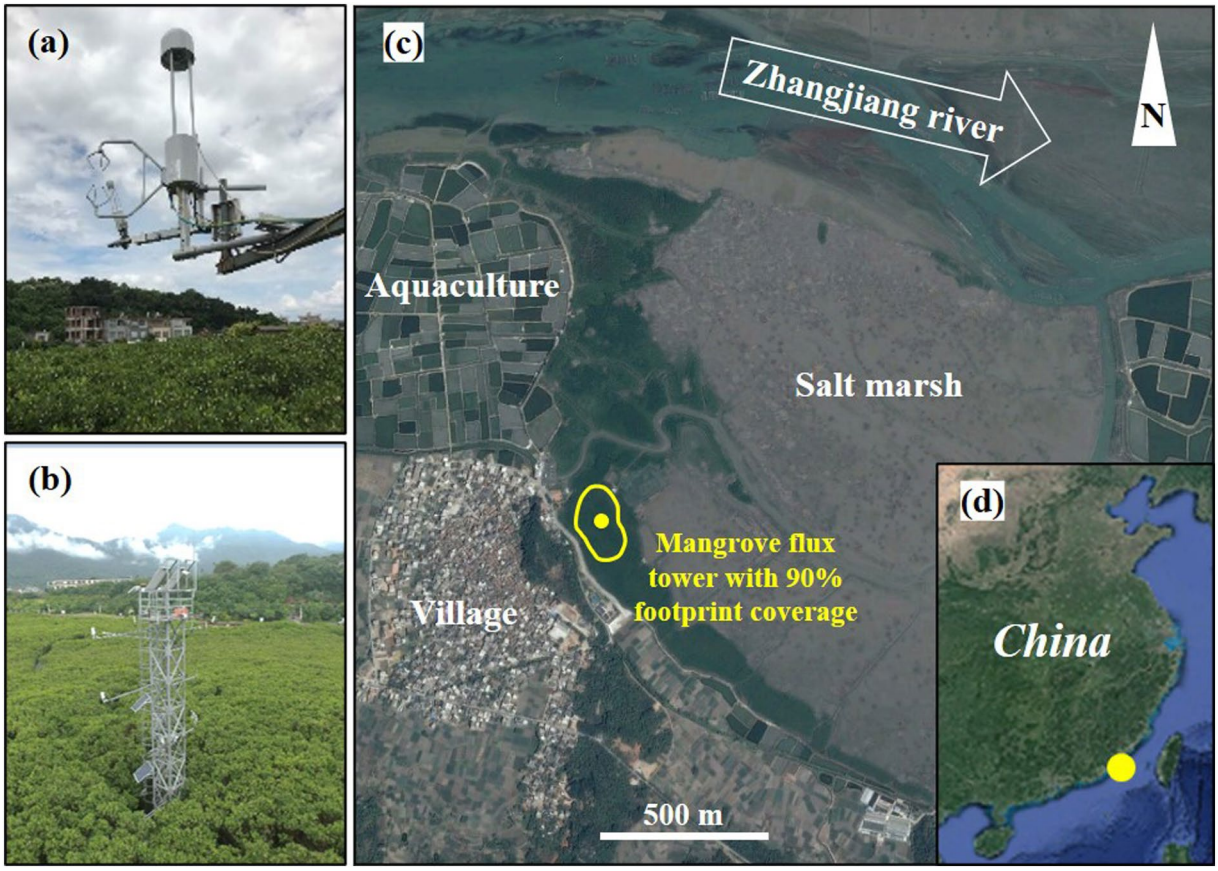

Figure 1. The greenhouse gas (GHG) eddy covariance system (a) installed on a flux tower (b) in a subtropical estuarine mangrove wetland (c: low-tide landscape with flux tower and its 90% footprint coverage marked by yellow dot and circle, respectively) of Southeast China (d).

deployed near sediment surface and another (CS106 barometer, Vaisala) deployed on flux tower. Raw time series measurements of GHG and meteorological variables mentioned above were recorded by two in-situ data loggers (CR1000 and CR3000, Campbell Scientific, Inc.) for subsequent data collection and processing. In addition, monthly river discharge data were collected from a hydrological station of Zhangjiang river ~10 km upstream from the study site to examine the impact of river discharge on surface water salinity at the flux tower.

2.3. Flux Data Processing

Data pre-processing including necessary flux calculations and quality controls (Zhu, Hou, et al., 2019; Zhu, Qin, et al., 2019) were applied to raw 10-Hz EC data to produce 30-min time series of NEE and NME, using the EddyPro6.1 software (Li-COR Inc.). Flux data were removed when rainfall occurred or atmospheric mixing was insufficient, determined by the friction velocity (u^*) threshold approach (Reichstein et al., 2005) with $u^* > 0.15$ m s^{-1} used in this study. Storage fluxes estimated from a single-point concentration profile approach were considered to correct flux data. The steady state test and the developed turbulent conditions test were applied to attain quality flags of fluxes following Mauder et al. (2013) (0-1-2 system: "0" for the best quality fluxes, "1" for fluxes suitable for general analysis, and "2" for poor fluxes that should be discarded), and the fluxes with the flag of 2 were excluded from further analysis. Methane-related flux data were also removed when the mirrors of LI7700 were contaminated, that is, the relative signal strength indicator <20% (to maintain a good signal, lower mirror was cleaned automatically via an in-line pumping system, while upper mirror was manually cleaned twice a month). These quality control procedures and other system failures led to data gaps with different durations (a large gap occurred in November and December 2019 due

to a power supply issue). Over the study period from August 2019 to December 2020, the remaining valid data coverage was 54.1% for NEE and 58.0% for NME.

To examine mangrove GHG budgets, the time series of daily NEE and NME were gap filled. Following many previous EC studies (Li et al., 2018; Liu et al., 2020; Moffat et al., 2007), the artificial neural network (ANN) approach was applied in the gap-filling procedure. Specifically, the ANN models were developed by linking daily fluxes with driving variables including daily mean air temperature, 10-cm soil temperature, PAR, VPD, surface water salinity, and daily maximum surface water level. The whole data set with model target (NEE or NME) and inputs was divided into training (75%), validation (15%), and testing (15%) subsets to develop the ANN models, in which the correlation coefficients between model target and output for the whole data set were 0.92 and 0.84 for NEE and NME, respectively. Mangrove gross primary productivity (GPP) and ecosystem respiration (Re) were partitioned from 30-min NEE. Re was estimated from air temperature based on the fitted nighttime NEE-air temperature relationship (measurements were excluded from the fitting when sediment surface was inundated), and then GPP was calculated as the difference between daytime NEE and corresponding Re (Barr et al., 2013; Reichstein et al., 2005).

The comparison of radiative forcing impacts of CO_2 and CH_4 fluxes is not straightforward due to their different lifetimes and radiative efficiencies in the atmosphere. The net radiative forcing from NEE and NME is temporally dynamic with both magnitude and sign changing with the time horizon chosen for the comparison (Frolking et al., 2006; Neubauer, 2014). Instead of using the standard GWP metric assuming only a single pulse input, the net radiative forcing in this study was calculated using the sustained-flux global warming potential (SGWP) metric (Liu et al., 2020; Neubauer & Megonigal, 2015), which in a more reasonable manner allows for a time series of sustained and variable gas fluxes. Despite that the dynamic behavior of net radiative forcing is a function of time horizon, the evaluation of net radiative forcing for several time horizons gives a simple indication. In this study, two commonly used time horizons (100-year and 20-year) were chosen to evaluate the net radiative forcing from NEE and NME, expressed as CO_2 equivalent (CO_2-eq.), using the values of 45 and 96 (Neubauer & Megonigal, 2015) to calculate SGWP of CH_4 for 100-year and 20-year time horizons, respectively.

2.4. Statistical Analysis

Considering the importance of rainfall in regulating salinity and GHG cycling, data were analyzed respectively for the dry season (October – March), the wet season (April – September), and the whole study period. The relationships between 30-min/daily GHG fluxes and other factors were fitted using non-linear or linear empirical curves. The non-linear dependence of daytime NEE on PAR was explored using the Michaelis-Menten light response curve (Michaelis & Menten, 1913): $\mathrm{NEE} = -\left(\varepsilon_m \times PAR \times P_m\right) / \left(\varepsilon_m \times PAR + P_m\right) + R_e$, where ε_m, P_m, and R_e denoted maximum light use efficiency, maximum photosynthesis capacity, and ecosystem respiration, respectively. The non-linear dependence of nighttime NEE on air temperature (T) was explored using the Lloyd-Taylor temperature response curve (Lloyd & Taylor, 1994): $\mathrm{NEE} = R_{ref} e^{E_0\left(1/\left(T_{ref}-T_0\right)-1/\left(T-T_0\right)\right)}$, where R_{ref}, E_0, T_{ref}, and T_0 denoted reference respiration, activation parameter, reference temperature (set as 10°C), temperature constant (set as −46.02°C), respectively. The temperature sensitivity Q_{10} (i.e., the rate of change in respiration as a consequence of increasing the temperature by 10°C) was also calculated from the fitted temperature response curves using 10°C as the base temperature: $Q_{10} = R_{20} / R_{10}$, where R_{20} and R_{10} denoted nighttime NEE at 20°C and 10°C, respectively. Linear dependences were assumed to examine the correlations including nighttime NEE-surface water salinity, NME-surface water salinity, NME-soil temperature, NME-GPP, and NME-Re. Standardized multiple regressions analyses were applied to further quantify the magnitude of relative importance, indicated by the absolute values of standardized regression coefficients, of major driving factors (PAR, air/soil temperature, salinity) in controlling daily NEE and NME. In this study, the sign convention in meteorology (i.e., the downward flux or sink is negative and the upward flux or source is positive) was used for indicating CO_2, CH_4, and GHG fluxes.

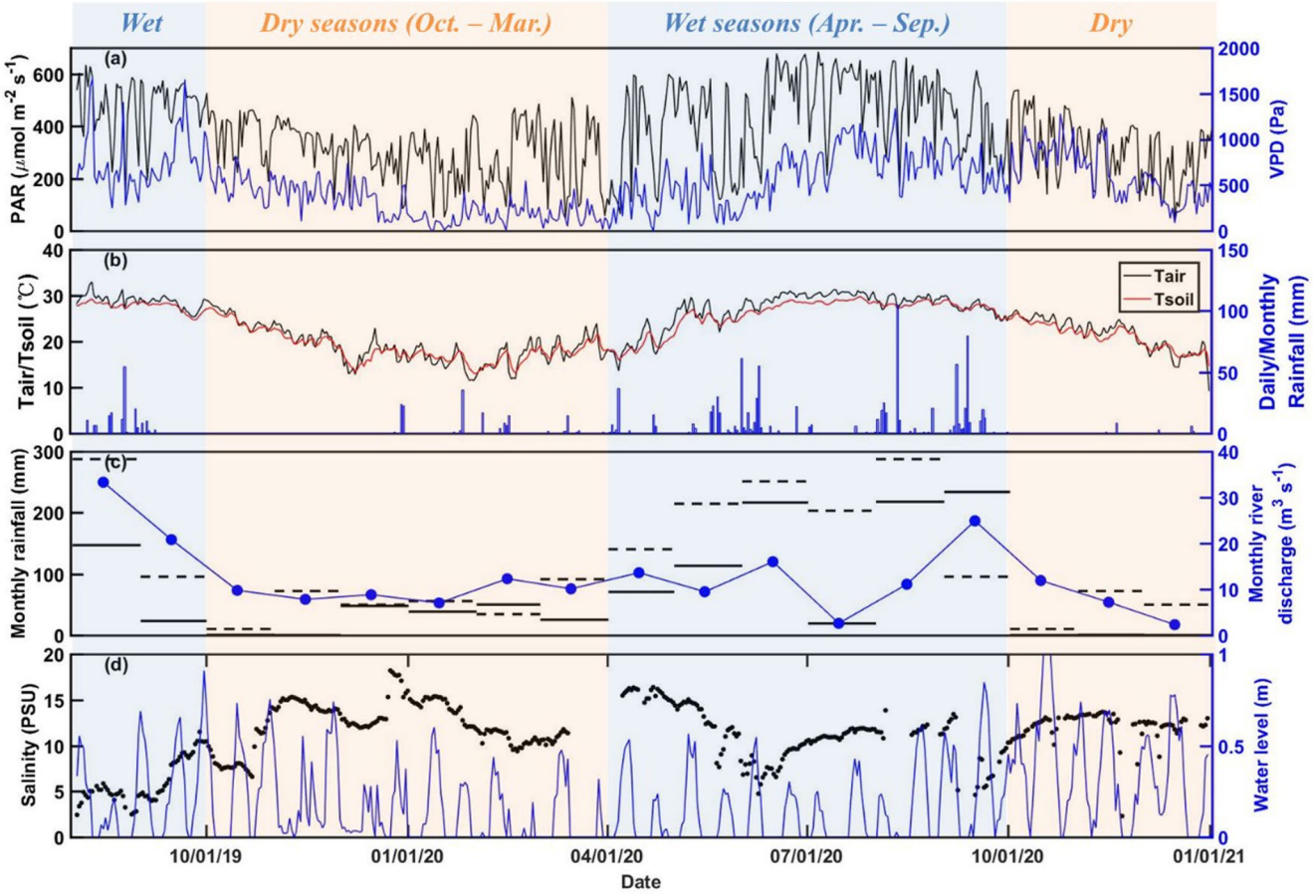

Figure 2. Temporal variations in daily meteorological and hydrological variables from August 2019 to December 2020, including (a) mean photosynthetically active radiation (PAR), mean vapor pressure deficit (VPD), (b) mean air temperature (Tair), mean 10-cm soil temperature (Tsoil), cumulative rainfall, (d) mean surface water salinity, and maximum surface water level. Monthly cumulative rainfall (horizontal solid lines) and corresponding multi-year average (2011–2019; horizontal dashed lines) and monthly river discharge are also shown (c).

3. Results

3.1. Temporal Variations in Meteorological and Hydrological Measurements

Over the study period, the time series of daily PAR showed strong short-term variations as a result of frequent cloudy conditions in this coastal mangrove site (Figure 2a). At seasonal time scale, daily PAR over the dry season (mean ± standard deviation: 305.1 ± 116.4 μmol m^{-2} s^{-1}) was on average lower than that over the wet season (452.2 ± 153.6 μmol m^{-2} s^{-1}). The time series of daily VPD showed similar seasonal variation pattern as PAR, with lower mean daily VPD over the dry season (403.0 ± 278.5 Pa) than that over the wet season (625.2 ± 306.7 Pa) (Figure 2a). Daily air and 10-cm soil temperature shared similar seasonal variation pattern with air temperature most of time higher (0.69°C on average) than soil temperature (Figure 2b). For air temperature, daily value varied from 9.2°C to 33.0°C with the lowest and highest values occurring in December of 2020 and August of 2019, respectively. Daily rainfall showed a large seasonal difference with most (85.0%) of rainfall occurring within the wet season and the remaining within the dry season (Figure 2b). In comparison with multi-year monthly average (based on daily rainfall measurements over 2011–2019 from a standard meteorological station of China Meteorological Administration, ~10 km away from this mangrove site), monthly rainfall was less in almost all months over the study period (except February and September of 2020; Figure 2c). In particular, obviously reduced rainfall occurred in spring (209.3 mm) and summer (453.6 mm) of 2020 than the multi-year average (446.3 and 741.9 mm). Monthly river discharge varied from 2.3 to 33.3 m^3 s^{-1} and was statistically ($p < 0.05$, hereinafter same) positively correlated with monthly rainfall (Figure 3c). Daily maximum surface water level changed over the study period

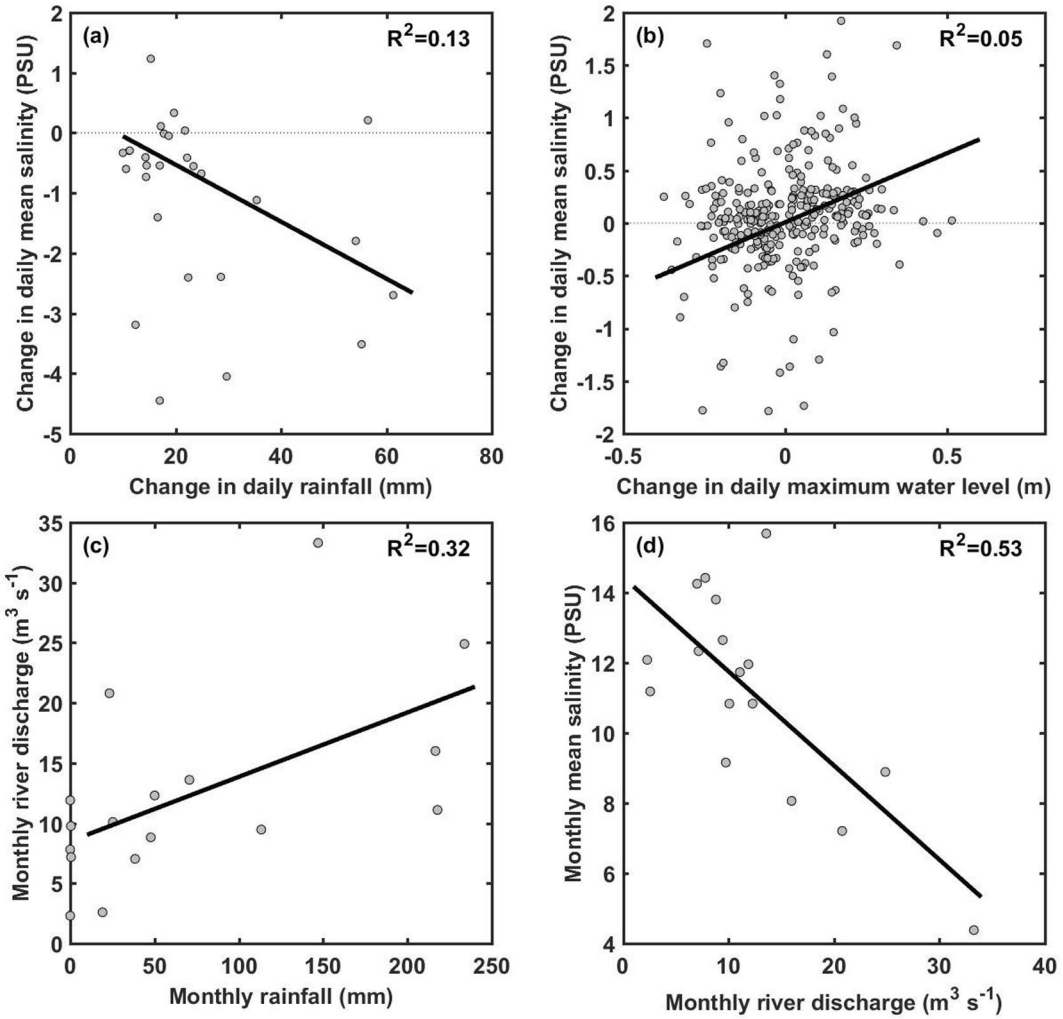

Figure 3. Change in daily mean surface water salinity within two consecutive days as a function of (a) change in daily cumulative rainfall and (b) change in daily maximum surface water level (note only those with rainfall <10 mm and >10 mm in two consecutive days are included). The rainfall-discharge and discharge-salinity relationships at monthly time scale are also shown (c) and (d). Fitted lines on these relationships are all statistically significant ($p < 0.05$).

with a biweekly cycle, and the tidal water height (up to ~1 m) peaked in autumn over the year (Figure 2d). Fluctuating with rainfall events, daily surface water salinity ranged from 2.4 to 18.2 PSU and was on average lower in the wet season (9.8 ± 3.4 PSU) than the dry season (12.4 ± 2.2 PSU). At daily time scale, surface water salinity declined with increasing daily rainfall (Figure 3a) and was statistically positively correlated with increasing daily maximum surface water level (Figure 3b). At monthly time scale, surface water salinity was statistically negatively correlated with increasing river discharge (Figure 3d).

3.2. Temporal Variations in Mangrove GHG Fluxes

Mean diurnal variation of 30-min mangrove NEE showed a distinct diurnal pattern with weak nighttime CO_2 sources (positive values; averaged at 2.77 μmol m^{-2} s^{-1}) and strong daytime CO_2 sinks (negative values; up to −14.03 μmol m^{-2} s^{-1} at noon) (Figures 4c and 4d). On average, daily ecosystem respiration (Re) in this mangrove was estimated to ~3.13 g CO_2-C m^{-2} day^{-1}, which offset 52.0% of daily ecosystem photosynthesis (GPP = ~ −6.02 g CO_2-C m^{-2} day^{-1}). There was no obvious difference in diurnal variations of NEE between the dry and wet seasons, although the dry season had a stronger peak sink and a narrower photosynthetic duration. In contrast, mangrove NME showed a weak diurnal pattern with one peak occurring in the late afternoon and two troughs occurring at hours before and after noon, respectively (Figures 4e and 4f). In

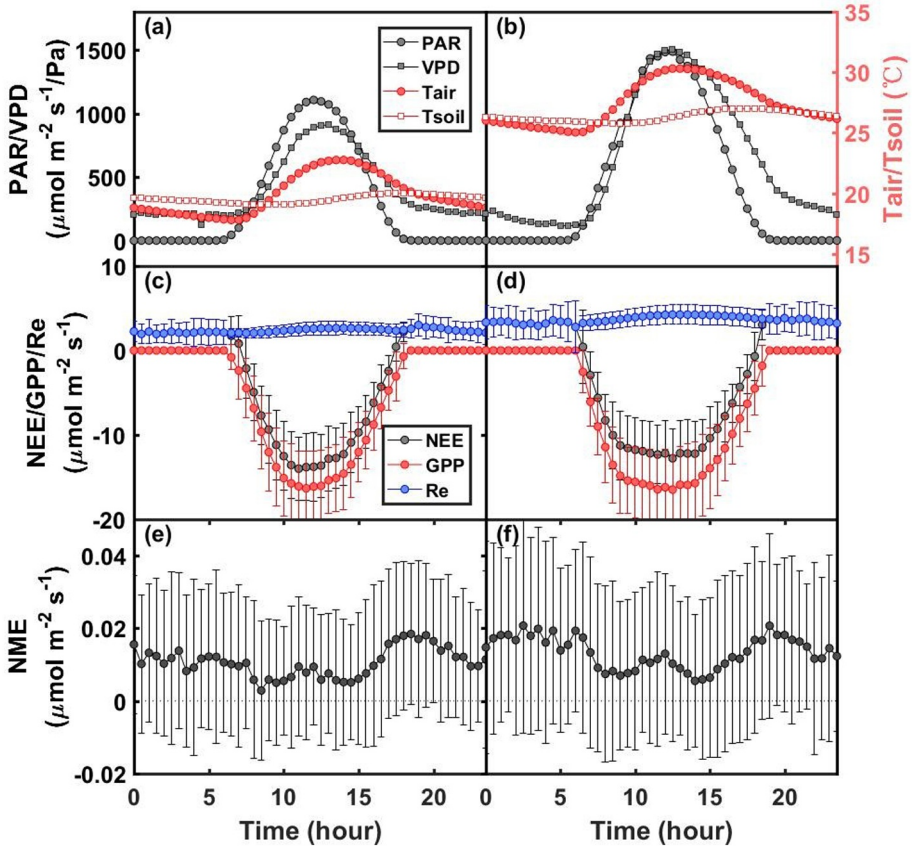

Figure 4. Diurnal variations in 30-min (a), (b) meteorological variables (c), (d) net ecosystem CO_2 exchange (NEE), and (e), (f) net ecosystem CH_4 exchange (NME) in the dry (October ~ March; left panel) and wet (April ~ September; right panel) seasons. PAR: photosynthetically active radiation; VPD: vapor pressure deficit; Tair: air temperature; Tsoil: 10-cm soil temperature. Error bars denote standard deviations of 30-min NEE and NME.

terms of mean diurnal variation, this mangrove acted consistent CH_4 sources over the day ranging from 0.0039 to 0.0194 μmol m^{-2} s^{-1}, although the deviations of 30-min NME across days were proportionately larger than that of 30-min NEE.

Daily cumulative values of NEE in this mangrove were consistently negative but fluctuated over the study period with the strongest CO_2 sink up to −5.39 g CO_2-C m^{-2} day^{-1}, and monthly mean daily NEE varied from −2.24 to −3.55 g CO_2-C m^{-2} day^{-1} with obviously weaker CO_2 sink in summer and autumn of 2020 (Figure 5a). Specifically, cumulative CO_2 sink over August ~ October of 2020 accounted for ~70% of the sink over the same period of 2019 (Figure 6a). Almost all daily cumulative values of NME in this mangrove were positive over the study period with daily NME ranging from −0.0195 to 0.0511 g CH_4-C m^{-2} day^{-1} and monthly mean daily NME ranging from 0.0034 to 0.0282 g CH_4-C m^{-2} day^{-1} (Figure 5b). It is obvious that the CH_4 emissions over August ~ October were stronger than other months in both 2019 and 2020, and cumulative CH_4 emissions in these months of 2020 were only ~40% of those over the same period of 2019 (Figures 5 and 6b).

3.3. Environmental Drivers of Mangrove GHG Fluxes

Statistical analyses on the responses of 30-min/daily NEE to environmental factors (Figure 7) indicated that daytime NEE was mainly regulated by PAR with saturating CO_2 sink at high PAR (30-min: $y = -1.03x / (0.051x + 20.26) + 2.92$; daily: $y = -1.37x / (0.10x + 13.7) + 2.04$), while nighttime NEE was positively and exponentially correlated with air temperature (30-min: $y = 1.39e^{3.96-220/(x+46.02)}$; daily: $y = 1.31e^{4.35-243/(x+46.02)}$) and negatively and linearly correlated with surface water salinity (30-min:

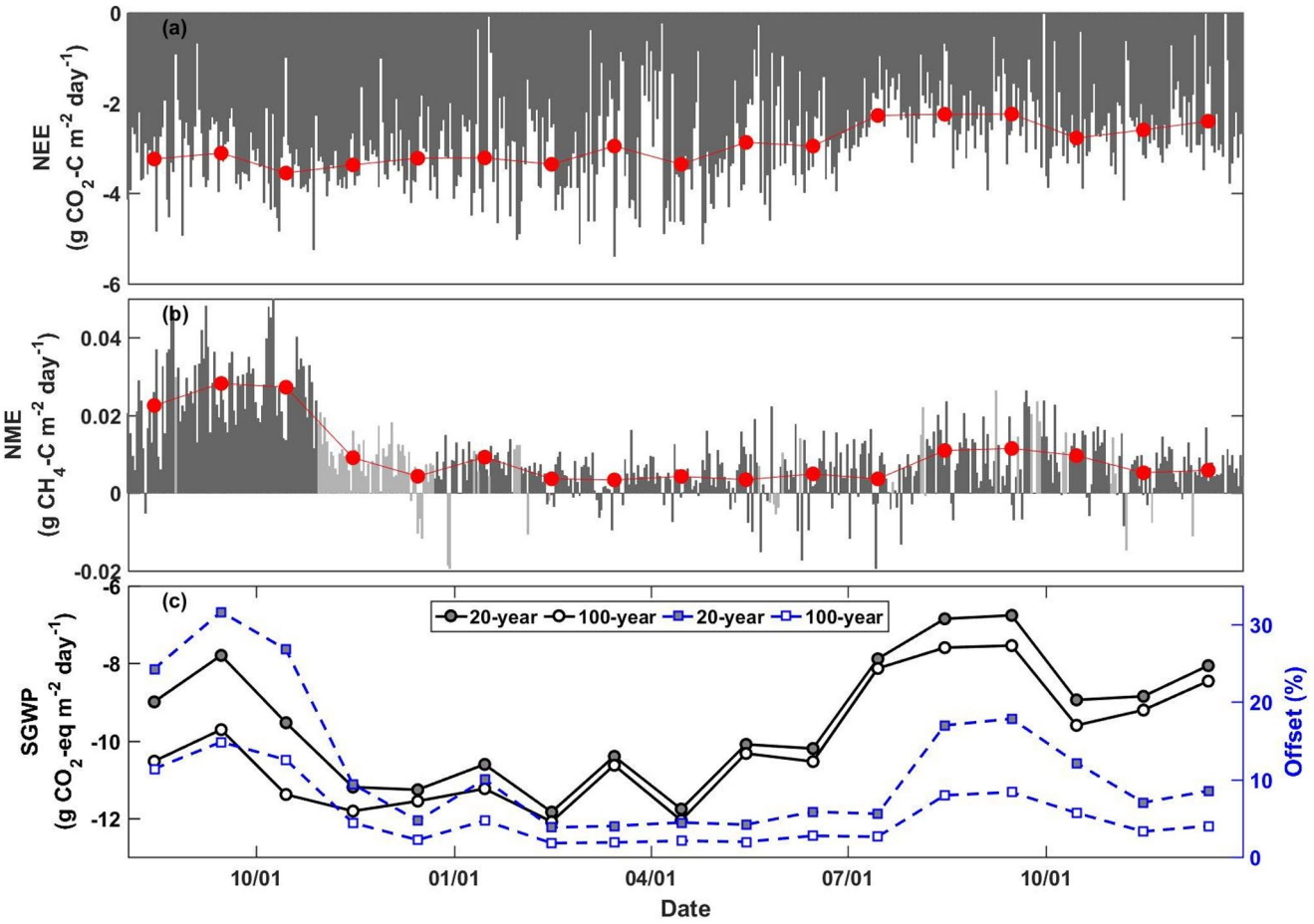

Figure 5. Temporal variations in daily (gray bars) and monthly (red dots) net ecosystem CO_2 (NEE) and CH_4 (NME) exchange from August 2019 to December 2020 (a), (b), where lighter gray bars denote the gap-filled daily values from the ANN model simulations. Monthly variations in SGWP and CH_4 offset potential are also shown (c) with the conversion values of 45 and 96 for 100-year and 20-year time horizons, respectively.

y = −0.12x + 4.18; daily: y = −0.14x + 4.50). The responses of NEE to these environmental factors differed between the dry and wet seasons. Maximum photosynthesis capacity (P_m) in the dry season (23.03 and 16.30 for 30-min and daily data, respectively) was larger than the wet season (19.96 and 13.10), while nighttime CO_2 source in the wet season was more sensitive to both air temperature (Q_{10} of the dry and wet seasons for 30-min data: 1.49 vs. 2.04; for daily data: 1.54 vs. 2.20) and surface water salinity (fitted linear slope of the dry and wet seasons for 30-min data: −0.044 vs. −0.082; for daily data: −0.059 vs. −0.10). Standardized multiple regression analysis between daily NEE and major driving factors (PAR, air temperature, and salinity) indicated that the relative importance of PAR (standardized regression coefficient of −0.43) and air temperature (0.40) were comparable and higher than salinity (0.06).

Statistical analyses on the responses of 30-min/daily NME to environmental factors (Figure 8) indicated that NME were negatively and positively correlated with surface water salinity (30-min: y = −0.0016x + 0.029; daily: y = −0.0015x + 0.027) and soil temperature (30-min: y = 0.0011x − 0.014; daily: y = 0.0006x − 0.0049), respectively. The responses of NME to these two factors tended to be more sensitive in the dry season (fitted linear NME-salinity slopes for 30-min and daily data: −0.0020 and −0.0017; NME-temperature slopes for 30-min and daily data: 0.0020 and 0.0013) than the wet season (NME-salinity slopes for 30-min and daily data: −0.0014 and −0.0017; NME-temperature slopes for 30-min and daily data: 0.0013 and 0.0007). It was also found that daily NME were negatively and positively correlated with GPP (y = −0.0022x − 0.0034) and Re (y = 0.0027x + 0.0023), respectively. Standardized multiple regression analysis between daily NME and major driving factors (PAR, soil temperature, and salinity) indicated that the relative importance of salinity (standardized regression coefficient of 0.32) was higher than soil temperature (0.20) and PAR (0.06).

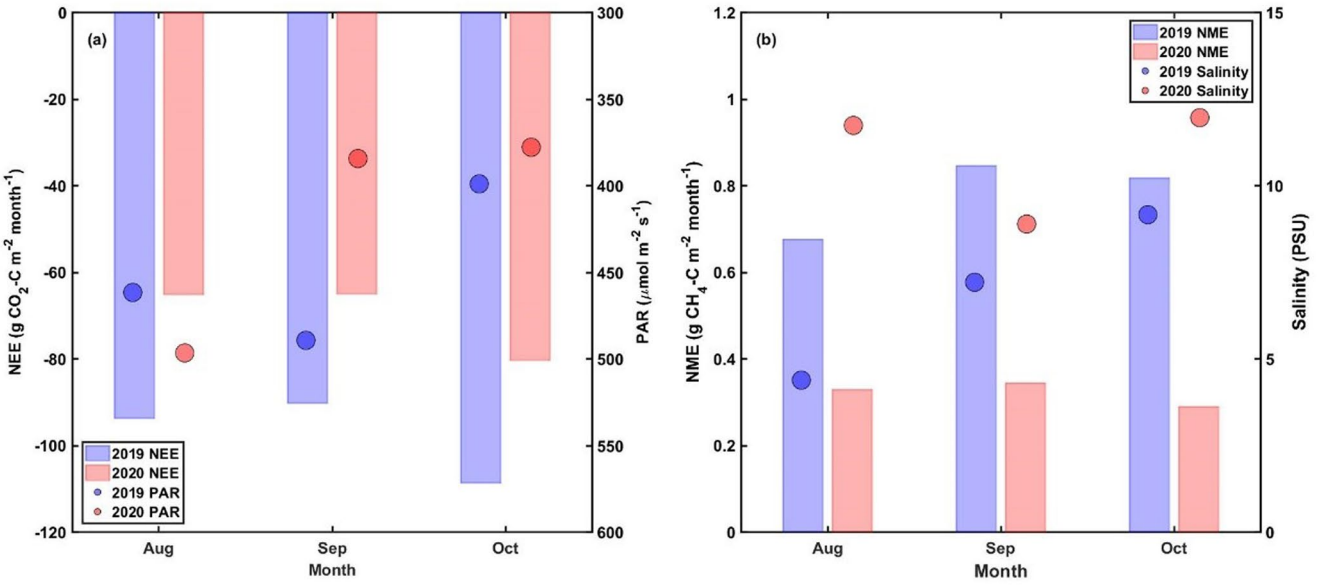

Figure 6. Comparison of monthly cumulative (a) net ecosystem CO_2 exchange (NEE) and (b) net ecosystem CH_4 exchange (NME) during August ~ October between 2019 and 2020. Monthly mean photosynthetically active radiation (PAR) and surface water salinity are also shown for NEE and NME, respectively.

3.4. Net GHG Balance

At monthly time scale, the SGWP-based net radiative forcing of this mangrove over the study period were estimated to −7.5 ~ −12.1 g CO_2-eq. m^{-2} day^{-1} (corresponding CH_4 offset potential: 1.8–14.8%) and −6.8 ~ −11.8 g CO_2-eq. m^{-2} day^{-1} (corresponding CH_4 offset potential: 3.8–31.6%) for 100-year and 20-year time horizons, respectively (Figure 5c). At annual time scale, this mangrove acted a CO_2 sink of −1,075.8 g CO_2-C m^{-2} $year^{-1}$ and a CH_4 source of 3.1 g CH_4-C m^{-2} $year^{-1}$, leading to a 100-year SGWP of −3,761.9 g CO_2-eq. m^{-2} $year^{-1}$ or a 20-year SGWP of −3,554.9 g CO_2-eq. m^{-2} $year^{-1}$ (here 1 g CO_2-C = 3.67 g CO_2-eq.). Net radiative forcing was dominated by the radiative cooling effect from CO_2 sink for all months over the study period. The radiative warming effect from CH_4 source annually offset 4.6% (100-year) or 9.8% (20-year) of the CO_2-induced SGWP.

4. Discussion

4.1. GHG Budgets and Temporal Variations

Consistent with previous mangrove EC studies (Barr et al., 2010; Leopold et al., 2016; Liu & Lai, 2019), NEE in this mangrove shows a distinct diurnal variation pattern and the magnitude of nighttime CO_2 source is much lower than daytime CO_2 sink. In mangrove ecosystems, the percentage of respiratory costs of assimilated carbon is generally small mainly due to low Re associated with saturated and anoxic sediments (Barr et al., 2010). Daily Re in this mangrove, ~3.13 g CO_2-C m^{-2} day^{-1}, is at the low end of the range reported by EC studies in terrestrial ecosystems, 1–7 g CO_2-C m^{-2} day^{-1} (Falge et al., 2002). The seasonal variation of daily NEE suggests that this subtropical mangrove has weaker CO_2 sink capacity in summer and autumn, which is similar to the finding in another subtropical mangrove wetland of China (Liu & Lai, 2019). With low Re and year-round productivity, this subtropical mangrove acts a high annual CO_2 sink of −1,075.8 g CO_2-C m^{-2} $year^{-1}$ over the study period, which is at the high end of the range, −74 ~ −1,170 g CO_2-C m^{-2} $year^{-1}$, reported by previous mangrove EC studies (Barr et al., 2010; Cui et al., 2018; Leopold et al., 2016; Liu & Lai, 2019).

The diurnal variation of NME in this mangrove is not clear, which can be explained by the fact that the magnitude of NME is co-regulated by more processes associated with CH_4 production, oxidation, and transport (Bridgham et al., 2013). The NME peaks in the late afternoon (at 5–7 p.m.; Figures 4e and 4f) since strong CH_4 production and weak CH_4 oxidation might occur simultaneously at these hours when soil temperature

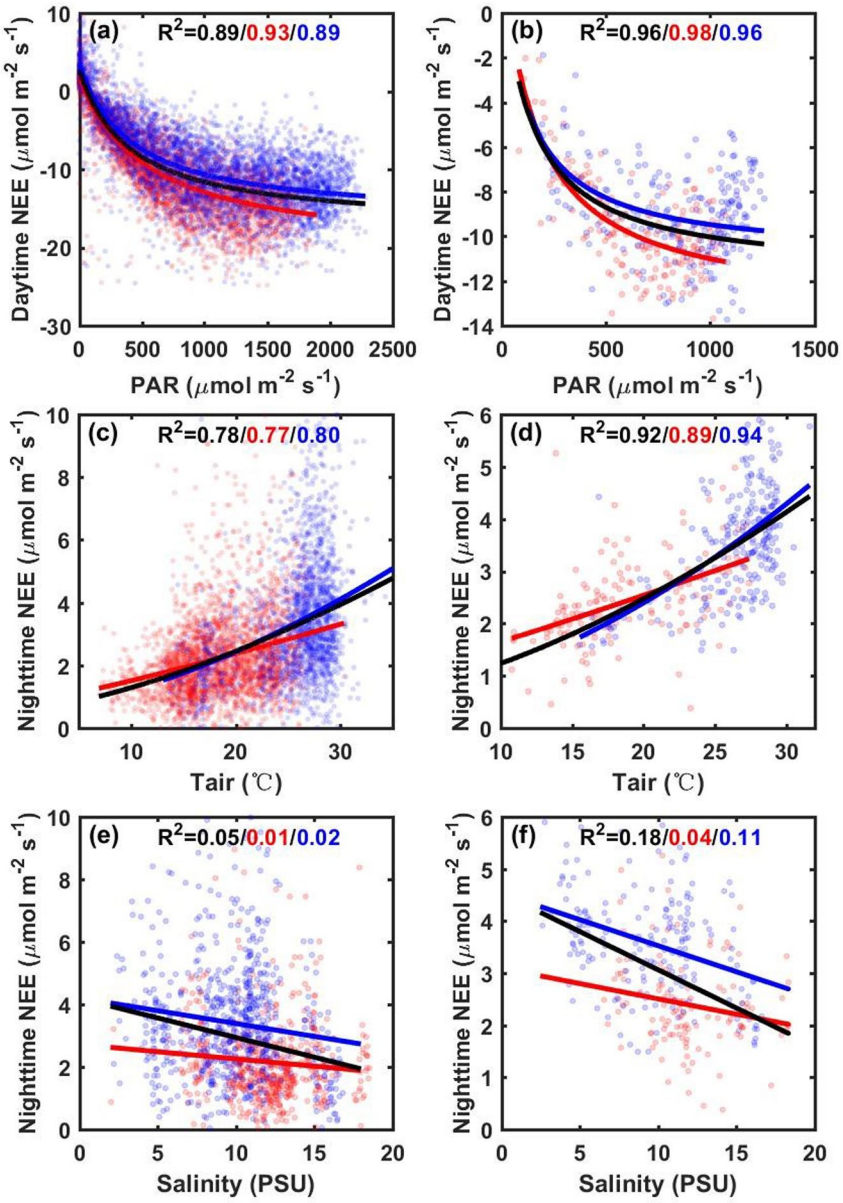

Figure 7. Daytime/nighttime net ecosystem CO_2 exchange (NEE) as a function of photosynthetically active radiation (PAR), air temperature (Tair), and surface water salinity. Both 30-min (left panel) and daily (right panel) average are shown for the relationships. Red and blue dots and corresponding fitting curves denote the data in the dry (October ~ March) and wet (April ~ September) seasons, respectively. Black fitting curves denote the relationships using the whole data set. Fitted lines on these relationships are all statistically significant ($p < 0.05$).

peaks over the day and PAR almost vanishes (Figures 4a and 4b). Daytime photosynthesis can improve oxygen availability in mangrove root zones via oxygen diffusion through the pneumatophores and thus stimulates CH_4 oxidation (Kitaya et al., 2002; Timmers et al., 2017), which might explain why daytime NME is often lower than nighttime NME (Figures 4e and 4f). The abrupt increase in NME at noon might be caused by a temporary shutdown of oxygen diffusion due to midday depression of plant photosynthesis (Xu & Shen, 1996). The seasonal variation of CH_4 emissions from this mangrove, showing higher emissions in the wet season than the dry season, is consistent with the findings in other subtropical/tropical wetlands with similar seasonal variations in temperature and rainfall (Dalmagro et al., 2019; Philipp et al., 2017; Tang et al., 2018). In comparison with a recent EC study on mangrove NME (Liu et al., 2020), daily NME of this mangrove shows less noticeable seasonal variation pattern. The difference in the seasonality may

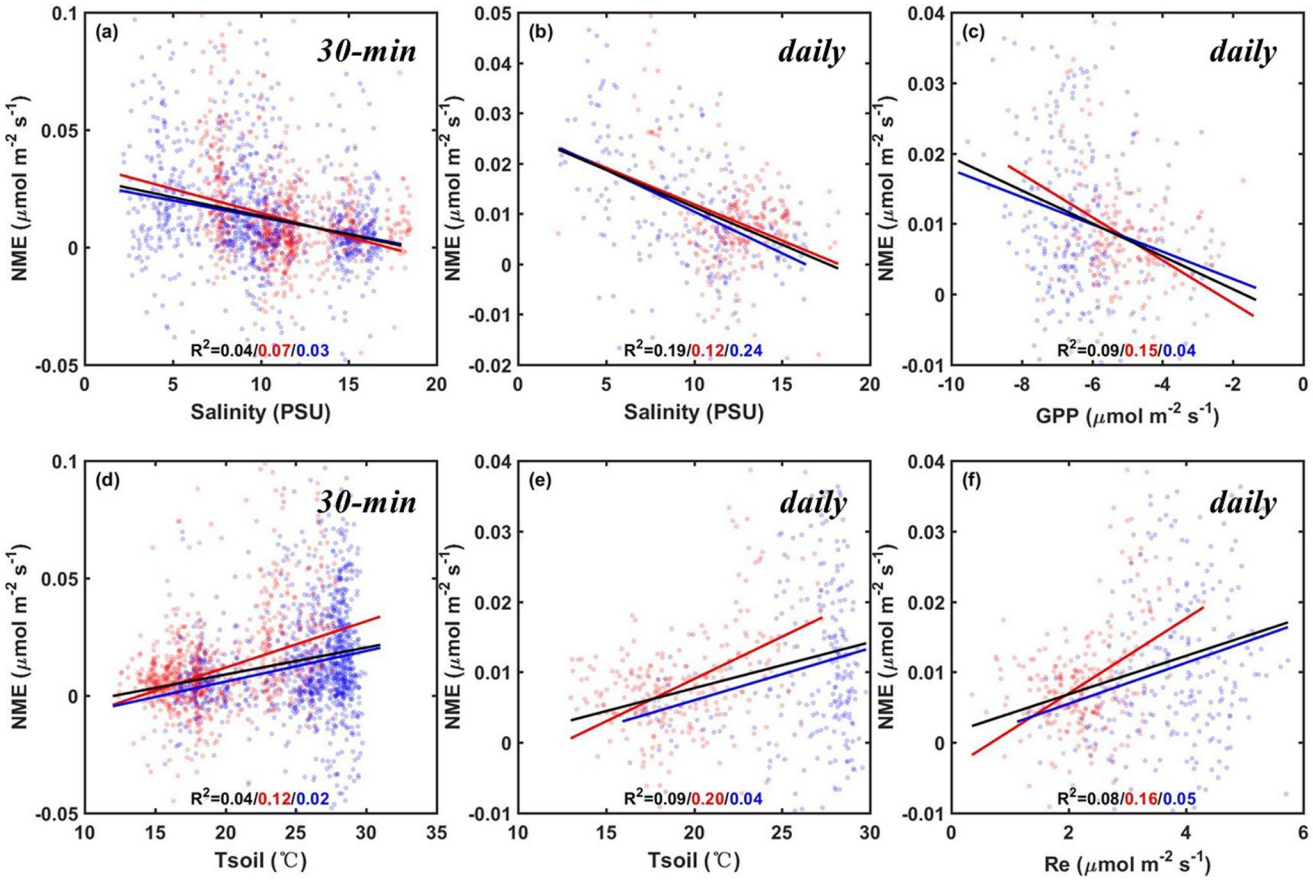

Figure 8. Net ecosystem CH_4 exchange (NME) as a function of (a) 30-min and (b) daily surface water salinity and (d) 30-min and (e) daily 10-cm soil temperature (Tsoil). Red and blue dots and corresponding fitting curves denote the data in the dry (October ~ March) and wet (April ~ September) seasons, respectively. Black fitting curves denote the relationships using the whole data set. Fitted lines on these relationships are all statistically significant ($p < 0.05$).

be explained by the following reasons: (a) the salinity in this mangrove has smaller seasonal variation and larger day-to-day variation regulated by rainfall events (Figure 2d), while the salinity of Liu et al. (2020) shows much stronger seasonality likely due to the fact that ~90% of the annual rainfall occurs in summer in that study; (b) the salinity condition of Liu et al. (2020) is presumably much more regulated by freshwater input since the magnitude of the annual discharge of Pearl River is two or three orders higher than that of Zhangjiang river; (c) the reduction of CH_4 emissions due to drought of 2020 also lead to weaker seasonal variation pattern of CH_4 emissions in this mangrove.

According to a synthesis study on chamber-based CH_4 efflux from undisturbed/disturbed mangrove sediments (Zheng et al., 2018), the magnitude of EC-based CH_4 emissions from this undisturbed (under strict protection by the national natural reserve) mangrove (0.0039–0.0194 μmol m^{-2} s^{-1} over the day) is generally higher than those from other undisturbed mangrove sediments (median of 0.001 μmol m^{-2} s^{-1}) and even comparable with those from disturbed mangrove sediments (median of 0.015 μmol m^{-2} s^{-1}). Annual CH_4 budget (3.1 g CH_4-C m^{-2} $year^{-1}$) in this mangrove is generally lower than those budgets (average of 16.5 g CH_4-C m^{-2} $year^{-1}$) in inland wetlands (Knox et al., 2019), while it is 2–3 times of the median mangrove CH_4 budget (1.2 g CH_4-C m^{-2} $year^{-1}$) reported by another synthesis study on CH_4 emissions with multiple measuring techniques from shallow vegetated coastal ecosystems (Al-Haj & Fulweiler, 2020). The discrepancies of CH_4 flux among these studies could mainly result from the differences in the spatial and temporal coverage of various flux measuring techniques (Krauss et al., 2016). In comparison with Liu et al. (2020), another EC-based CH_4 study in subtropical mangroves, annual CH_4 emissions from this mangrove is only around one-quarter of theirs. This discrepancy may be attributed to the difference in site-dependent tidal and climate conditions: (a) the mangrove in this site experiences a shorter mean daily inundation duration

(~5% of time) in comparison with Liu et al. (2020) (~12%); (b) the salinity in this site is usually higher than that of Liu et al. (2020) especially in summer (~10 vs. ~3 PSU); (c) the amount of annual rainfall in this site during the studying period is much lower than that of Liu et al. (2020) (~1,000 vs. ~2,000 mm); and (d) seasonal rainfall is relatively more evenly distributed in this mangrove, while for Liu et al. (2020) ~90% of the rainfall occurs in summer.

4.2. Environmental Controls of GHG Budgets

Reductions of both CO_2 sink and CH_4 source occur in summer and autumn of 2020 in comparison with 2019, mostly due to the difference in PAR and salinity conditions. By comparing the period of August ~ October between 2019 and 2020 (Figure 6), reduction of CO_2 sink in 2020 is mainly attributed to the combination of lower PAR and drought-induced salinity enhancement, while reduction of CH_4 source is mainly attributed to enhanced salinity. There is no obvious difference in monthly soil temperature (0.3%, 0.2%, and 2.7% difference for these months) between 2019 and 2020 (Figure 2b). In contrast, rainfall in spring and summer of 2020 is only 56% of the multi-year average in this mangrove, and this severe drought results in overall higher salinity level in the following months (Figure 6b), which weakens CO_2 and CH_4 cycling. This important asynchronous process or lagged effect has also been identified in previous studies interpreting continuous ecosystem-scale GHG measurements (Knox et al., 2018; Sturtevant et al., 2016).

The inhibitory effect of salinity stress on mangrove growth has been well confirmed by previous studies (Alongi, 2009; Takemura et al., 2000). Despite that the correlation between salinity and daytime NEE is not statistically significant (data not shown), the salinity stress on GPP in this mangrove might be overwhelmed by the influence of PAR. The influence of salinity stress on NME found in this mangrove (Figures 6b, 8a, and 8b) supports the well-known notion that salinity is the key control of CH_4 emissions in mangroves (Al-Haj & Fulweiler, 2020; Knox et al., 2019). A threshold of ~18 PSU can be identified from the fitted linear salinity-NME relationship (Figures 8a and 8b), in which mangrove CH_4 emissions vanish with salinity level exceeding this threshold. This salinity threshold is recommended by IPCC to determine if mangrove CH_4 emissions should be considered in GHG inventory (Crooks, 2014), and also equivalent to the threshold associated with significant lower CH_4 emissions in tidal marshes (Poffenbarger et al., 2011). The statistically significant correlations between NME and GPP (Figure 8c) suggests that weaker CO_2 sink in summer and autumn of 2020 might be another important factor responsible for the reduction of NME. The link between NME and GPP has been demonstrated by many of previous studies (Hatala et al., 2012; Sturtevant et al., 2016; Whiting & Chanton, 1993), since low photosynthesis can limit the availability of labile substrate for methanogenesis (Bridgham et al., 2013).

4.3. Net Radiative Forcing

The consistent negative SGWP over the study period using either 100-year or 20-year time horizon confirms the climate benefits of mangroves in mitigating GHG emissions. The radiative warming effect from NME in this mangrove has the potential to offset 4.6% (or 9.8%) of the radiative cooling effect from NEE using the 100-year (or 20-year) SGWP metric. The CH_4 offset potentials of this mangrove are relatively low, being about half of those (10% or 22%; converted values using the same metric and time horizons as in this study) reported by a global synthesis study (Rosentreter et al., 2018b) and one fifth of those (24% or 52%) reported by another mangrove EC-based GHG study (Liu et al., 2020). Although it might be impossible to fully interpret the differences among studies due to various definitions of offset potentials and site-dependent biotic/abiotic factors, here are some aspects to mention. First, instead of using NEE-based CO_2 sink for estimating CH_4 offset potential in this study, Rosentreter et al. (2018b) uses sediment carbon burial-based CO_2 sink (smaller than NEE-based one that includes both buried and tide-exported carbon), and thus our estimation of CH_4 offset potential should be by definition lower than theirs. Second, in comparison with Rosentreter et al. (2018b) assuming a 50% daily inundation duration, this mangrove has a much shorter daily inundation duration (~5% of time), which could lead to lower CH_4 emissions and its offset potential. Third, in relation to Liu et al. (2020), the obviously lower CH_4 offset potential of this mangrove results from a stronger CO_2 sink (−1,075.8 vs. −782.3 g CO_2-C m^{-2} $year^{-1}$) and a weaker CH_4 source (3.1 vs. 11.7 g CH_4-C m^{-2} $year^{-1}$), which are mostly likely attributed to the difference in annual rainfall (~1,000 vs. ~2,000 mm) since more rainfall usually accompanies with less PAR (weaker CO_2 sink) and lower salinity (stronger CH_4 source).

In fact, drought-induced salinity enhancement in 2020 in this mangrove reduces both CO_2 sink and CH_4 source with a proportionately larger reduction in the latter, leading to a lower CH_4 offset potential. In particular, the averaged surface water salinity over August ~ October of 2020 (10.9 PSU) is more than 50% higher than that over the same period of 2019 (6.9 PSU) (Figure 6b). Correspondingly, the CH_4 offset potential over August ~ October of 2020%, 7.4% (15.7%) on a 100-year (20-year) time horizon, is obviously lower than that over the same period of 2019%, 12.9% (27.6%) (Figure 5c). The contrasting GHG budgets between 2019 and 2020 suggest that drought-induced salinity enhancement weakens mangrove GHG cycling and the CH_4 offset potential.

The strong seasonal variations in monthly CH_4 offset potential in this mangrove (e.g., the highest offset potential is ~8 times larger than the lowest one; Figure 5c) reflect the differential environmental controls of NEE and NME, which implies that long-term continuous GHG flux measurements are highly necessary to accurately assess mangrove GHG budgets and its net radiative forcing. Although both NME and nighttime NEE are affected by temperature and salinity, their sensitivities differ between the dry and wet seasons with stronger sensitivity of NME (nighttime NEE) in the dry (wet) season. This implies that the future changes in the seasonality of climate conditions such as seasonal distribution of rainfall (Collins et al., 2013) may exert differential effects on mangrove NEE and NME as well as their net radiative forcing.

4.4. Limitations and Uncertainties

The analyses of mangrove GHG budgets and their environmental controls in this study suffer from several limitation and uncertainties. First, due to the lack of long-term continuous measurements of ecosystem-level nitrous oxide (N_2O) flux, N_2O is not considered in assessing mangrove GHG budgets and its radiative forcing in this study. Despite that mangroves are often reported as a minor N_2O source or even a sink (Chen et al., 2010; Maher et al., 2016), future research is needed to take into account N_2O flux given that the radiative efficiency of N_2O is 270 times higher than CO_2 over a 100-year time horizon (Neubauer & Megonigal, 2015) and the magnitude of N_2O flux could be well stimulated by anthropogenic eutrophication (Chauhan et al., 2015; Kreuzwieser et al., 2003). Second, a portion of produced CO_2 and CH_4 in mangroves can be exported via tidal activities (Alongi, 2014; Call et al., 2015) but cannot be captured by EC measurements, and thus EC-based estimations of GHG budgets and CH_4 offset potential in mangroves might bias to a certain extent. Future research in assessing the contribution of horizontal GHG transport is needed to reduce this uncertainty. Third, surface water salinity is not necessarily equivalent to subsurface porewater salinity since they often differ in both the magnitude and temporal variation (Lara & Cohen, 2006). Mangrove GHG cycling is presumably more related with subsurface porewater salinity, and thus the analyses with surface water salinity in this study might not accurately reflect physiological salinity controls on mangrove GHG cycling. Further analyses should be conducted in future when long-term measurement of subsurface porewater salinity is available. Fourthly, deep soil temperature could exert a more important effect on CH_4 emissions than surface soil temperature (Liu et al., 2020), given that methanogenic archaea might be outcompeted down the thermodynamic ladder and expected to occur at greater soil depths in mangrove sediments (Alongi, 2009). We're short of continuous soil temperature measurements at deeper soil layers over the studying period, and future research with the availability of such measurements should be conducted to confirm the temperature-CH_4 relationships across soil layers. Fifthly, ecosystem-scale GHG fluxes are regulated by many non-linear and asynchronous processes, which often result in lagged effects between GHG flux (in particular for CH_4) and its abiotic/biotic controls at diurnal and seasonal scales (Rinne et al., 2018; Knox et al., 2019). Current 1.5-year measurement data set might be insufficient to analyze these lagged effects, and future research with multi-year continuous measurements is needed to better characterize these processes across time scales. Lastly, despite of its simplicity, the evaluation of SGWP with fixed time horizons as in this study cannot fully capture the dynamic behavior of net radiative forcing from NEE and NME. Further comparison of the radiative forcing of NEE and NME as a function of time horizons might be needed to provide a more comprehensive and informative assessment on the competing impacts of CO_2 and CH_4 fluxes at any time horizons or any time over the history of the wetland's development.

5. Conclusions

The EC-based long-term continuous measurements of ecosystem-level GHG fluxes suggested this subtropical estuarine mangrove acted as a CO_2 sink of −1,075.8 g CO_2-C m^{-2} $year^{-1}$ and a CH_4 source of 3.1 g CH_4-C m^{-2} $year^{-1}$ over the study period from August 2019 to December 2020, resulting in a net GHG sink of −3,761.9 and −3,554.9 g CO_2-eq. m^{-2} $year^{-1}$ (here 1 g CO_2-C = 3.67 g CO_2-eq.) expressed using the SGWP metric with 100-year and 20-year time horizons, respectively. This net radiative cooling effect was dominated by the year-round consistent CO_2 sink, and annually the CH_4-induced warming effect offset 4.6% (100-year) or 9.8% (20-year) of the CO_2-induced cooling effect. Both of NEE and NME showed strong temporal variations but with different diurnal and seasonal variation patterns. For mangrove NEE, daytime CO_2 sink was mainly regulated by PAR, while nighttime CO_2 source was positively and negatively correlated with air temperature and surface water salinity, respectively. For mangrove NME, CH_4 source was positively and negatively correlated with soil temperature and surface water salinity, respectively. Monthly CO_2 sink was stronger in colder spring and winter, while monthly CH_4 source was stronger in warmer summer and autumn. Drought-induced salinity enhancement, due to reduced rainfall and river discharge, weakened mangrove GHG cycling, leading to obviously weaker CO_2 sink and CH_4 source in summer and autumn of 2020 than the same period of 2019.

This study confirms that ecosystem-level CH_4 emissions from estuarine mangroves are not negligible and could substantially offset the radiative cooling effect from ecosystem CO_2 uptake. Strong temporal variations in mangrove GHG fluxes and their respective contributions to net radiative forcing highlights a strong necessity to conduct long-term continuous measurements of GHG fluxes. This study also confirms the critical roles of salinity and temperature in regulating mangrove GHG cycling, and future increases in temperature and salinity with expected global warming and sea level rise will likely reduce the radiative cooling effect and thus weaken the climate benefits of mangroves.

Conflicts of Interests

The authors declare no conflict of interest relevant to this study.

Data Availability Statement

The data necessary to reproduce key findings in this paper can be accessed at http://doi.org/10.5281/zenodo.4715772.

Acknowledgments
The authors thank Chunlin Wang, Yaqing Lu, Chenjuan Zheng and Guanmin Huang for their help in the field work and data processing. The authors thank the Zhangjiang Estuary Mangrove National Nature Reserve for its long-term support to our ecological research program. The authors also thank ChinaFLUX and the U.S.-China Carbon Consortium (USCCC) for helpful discussions and exchange of ideas. This study was supported by the National Natural Science Foundation of China (31600368), the National Key Research and Development Program of China (2017YFC0506102), the Natural Science Foundation of Fujian Province, China (2020J01112079), the Youth Innovation Foundation of Xiamen, China (3502Z20206038), the Fundamental Research Funds for the Central Universities of China (20720180118, 20720190104, 20720210075), the Key Laboratory of the Coastal and Wetland Ecosystems (WELRI201601) and the State Key Laboratory of Marine Environmental Science (MELRI1603).

References

Al-Haj, A. N., & Fulweiler, R. W. (2020). A synthesis of methane emissions from shallow vegetated coastal ecosystems. *Global Change Biology*, *26*(5), 2988–3005.

Alongi, D. M. (2009). The Energetics of Mangrove Forests (pp. e18–e19). Springer Netherlands.

Alongi, D. M. (2014). Carbon cycling and storage in mangrove forests. *Annual review of marine science*, *6*, 195–219. https://doi.org/10.1146/annurev-marine-010213-135020

Alongi, D. M., & Mukhopadhyay, S. K. (2014). Contribution of mangroves to coastal carbon cycling in low latitude seas. *Agricultural and Forest Meteorology*, *213*, 266–272.

Alvarado-Barrientos, M. S., López-Adame, H., Lazcano-Hernández, H. E., Arellano-Verdejo, J., & Hernández-Arana, H. A. (2020). Ecosystem-atmosphere exchange of CO_2, water and energy in a basin mangrove of the northeastern coast of the Yucatan Peninsula. *Journal of Geophysical Research: Biogeosciences*, e2020JG005811.

Baldocchi, D. (2019). How eddy covariance flux measurements have contributed to our understanding of Global Change Biology. *Global Change Biology*, *26*(1), 242–260.

Baldocchi, D., Falge, E., Gu, L., Olson, R., Hollinger, D., Running, S., et al. (2001). FLUXNET: A new tool to study the temporal and spatial variability of ecosystem–Scale carbon dioxide, water vapor, and energy flux densities. *Bulletin of the American Meteorological Society*, *82*(11), 2415–2434. https://doi.org/10.1175/1520-0477(2001)082<2415:fantts>2.3.co;2

Barr, J. G., Engel, V., Fuentes, J. D., Fuller, D. O., & Kwon, H. (2013). Modeling light use efficiency in a subtropical mangrove forest equipped with CO_2 eddy covariance. *Biogeosciences*, *10*(3), 2145–2158. https://doi.org/10.5194/bg-10-2145-2013

Barr, J. G., Engel, V., Joseph, F., Zieman, J. C., O'Halloran, T. L., Smith, T. J., et al. (2010). Controls on mangrove forest-atmosphere carbon dioxide exchanges in western Everglades National Park. *Journal of Geophysical Research: Biogeosciences*, *115*(G2). https://doi.org/10.1029/2009jg001186

Breithaupt, J. L., Smoak, J. M., Smith, T. J., III, Sanders, C. J., & Hoare, A. (2012). Organic carbon burial rates in mangrove sediments: Strengthening the global budget. *Global Biogeochemical Cycles*, *26*(3). https://doi.org/10.1029/2012gb004375

Bridgham, S. D., Cadillo-Quiroz, H., Keller, J. K., & Zhuang, Q. (2013). Methane emissions from wetlands: Biogeochemical, microbial, and modeling perspectives from local to global scales. *Global Change Biology*, *19*, 1325–1346. https://doi.org/10.1111/gcb.12131

Cabezas, A., Mitsch, W. J., MacDonnell, C., Zhang, L., Bydałek, F., & Lasso, A. (2018). Methane emissions from mangrove soils in hydrologically disturbed and reference mangrove tidal creeks in southwest Florida. *Ecological Engineering*, *114*, 57–65. https://doi.org/10.1016/j.ecoleng.2017.08.041

Call, M., Maher, D. T., Santos, I. R., Ruiz-Halpern, S., Mangion, P., Sanders, C. J., et al. (2015). Spatial and temporal variability of carbon dioxide and methane fluxes over semi-diurnal and spring-neap-spring timescales in a mangrove creek. *Geochimica et Cosmochimica Acta*, *150*, 211–225. https://doi.org/10.1016/j.gca.2014.11.023

Chauhan, R., Datta, A., Ramanathan, A. L., & Adhya, T. K. (2015). Factors influencing spatio-temporal variation of methane and nitrous oxide emission from a tropical mangrove of eastern coast of India. *Atmospheric Environment*, *107*, 95–106. https://doi.org/10.1016/j.atmosenv.2015.02.006

Chen, G., Tam, N., & Ye, Y. (2010). Summer fluxes of atmospheric greenhouse gases N_2O, CH_4 and CO_2 from mangrove soil in South China. *Science of the Total Environment*, *408*(13), 2761–2767. https://doi.org/10.1016/j.scitotenv.2010.03.007

Chen, H., Lu, W., Yan, G., Yang, S., & Lin, G. (2014). Typhoons exert significant but differential impacts on net ecosystem carbon exchange of subtropical mangrove forests in China. *Biogeosciences*, *11*(19), 5323–5333. https://doi.org/10.5194/bg-11-5323-2014

Collins, M., Knutti, R., Arblaster, J., Dufresne, J. L., Fichefet, T., Friedlingstein, P., et al. (2013). *Climate change 2013: The physical science basis. Contribution of working group I to the fifth assessment report of the intergovernmental panel on climate change*. Cambridge University Press.Long-term Climate Change: Projections, Commitments and Irreversibility.

Crooks, S. (2014). *2013 supplement to the 2006 IPCC guidelines for national greenhouse gas inventories: Wetlands*.

Cui, X. W., Liang, J., Lu, W., Chen, H., Liu, F., Lin, G., et al. (2018). Stronger ecosystem carbon sequestration potential of mangrove wetlands with respect to terrestrial forests in subtropical China. *Agricultural and Forest Meteorology*, *249*, 71–80. https://doi.org/10.1016/j.agrformet.2017.11.019

Dalmagro, H. J., Zanella de Arruda, P. H., Vourlitis, G. L., Lathuillière, M. J., de S. Nogueira, J., Couto, E. G., & Johnson, M. S. (2019). Radiative forcing of methane fluxes offsets net carbon dioxide uptake for a tropical flooded forest. *Global Change Biology*, *25*(6), 1967–1981. https://doi.org/10.1111/gcb.14615

Ewel, K., Twilley, R., & Ong, J. (1998). Different kinds of mangrove forests provide different goods and services. *Global Ecology and Biogeography Letters*, *7*(1), 83–94. https://doi.org/10.2307/2997700

Falge, E., Baldocchoi, D., Tenhunen, J., Aubinet, M., Bakwin, P., Berbigier, P., et al. (2002). Seasonality of ecosystem respiration and gross primary production as derived from FLUXNET measurements. *Agricultural and Forest Meteorology*, *113*(1–4), 53–74. https://doi.org/10.1016/s0168-1923(02)00102-8

Frolking, S., Roulnet, N., Fuglestvedt, J., (2006). How northern peatlands influence the Earth's radiative budget: Sustained methane emission versus sustained carbon sequestration. *Journal of Geophysical Research*, *111*(G1). https://doi.org/10.1029/2005jg000091

Giri, C., Ochieng, E., Tieszen, L. L., Zhu, Z., Singh, A., Loveland, T., et al. (2011). Status and distribution of mangrove forests of the world using earth observation satellite data. *Global Ecology and Biogeography*, *20*(1), 154–159. https://doi.org/10.1111/j.1466-8238.2010.00584.x

Hamilton, S. E., & Casey, D. (2016). Creation of a high spatio-temporal resolution global database of continuous mangrove forest cover for the 21st century (CGMFC-21). *Global Ecology and Biogeography*, *25*(6), 729–738. https://doi.org/10.1111/geb.12449

Hamilton, S. E., & Friess, D. A. (2018). Global carbon stocks and potential emissions due to mangrove deforestation from 2000 to 2012. *Nature Climate Change*, *8*(3), 240–244. https://doi.org/10.1038/s41558-018-0090-4

Hatala, J. A., Detto, M., & Baldocchi, D. D. (2012). Gross ecosystem photosynthesis causes a diurnal pattern in methane emission from rice. *Geophysical Research Letters*, *39*(6). https://doi.org/10.1029/2012gl051303

Howard, J., Sutton-Grier, A., Herr, D., Kleypas, J., Landis, E., Mcleod, E., et al. (2017). Clarifying the role of coastal and marine systems in climate mitigation. *Frontiers in Ecology and the Environment*, *15*(1), 42–50. https://doi.org/10.1002/fee.1451

Jeffrey, L. C., Reithmaier, G., Sippo, J. Z., Johnston, S. G., Tait, D. R., Harada, Y., & Maher, D. T. (2019). Are methane emissions from mangrove stems a cryptic carbon loss pathway? Insights from a catastrophic forest mortality. *New Phytologist*, *224*(1), 146–154. https://doi.org/10.1111/nph.15995

Keppler, F., Hamilton, J. T., Braß, M., & Röckmann, T. (2006). Methane emissions from terrestrial plants under aerobic conditions. *Nature*, *439*(7073), 187–191. https://doi.org/10.1038/nature04420

Kitaya, Y., Yabuki, K., Kiyota, M., Tani, A., Hirano, T., & Aiga, I., (2002). Gas exchange and oxygen concentration in pneumatophores and prop roots of four mangrove species. *Trees*, *16*(2–3), 155–158. https://doi.org/10.1007/s00468-002-0167-5

Knox, S. H., Jackson, R. B., Poulter, B., McNikol, G., Chouinard, E. F., Zhang, Z., et al. (2019). FLUXNET-CH_4 synthesis activity: Objectives, observations, and future directions. *Bulletin of the American Meteorological Society*, *100*(12), 2607–2632.

Knox, S. H., Windham-Myers, L., Anderson, F., Sturtevant, C., & Bergamaschi, B. (2018). Direct and indirect effects of tides on ecosystem-scale CO_2 exchange in a brackish tidal marsh in Northern California. *Journal of Geophysical Research Biogeosciences*.

Krauss, K. W., Holm, G. O., Perez, B. C., McWhorter, D. E., Cormier, N., Moss, R. F., et al. (2016). Component greenhouse gas fluxes and radiative balance from two deltaic marshes in Louisiana: Pairing chamber techniques and eddy covariance. *Journal of Geophysical Research: Biogeosciences*, *121*(6), 1503–1521. https://doi.org/10.1002/2015jg003224

Kreuzwieser, J., Buchholz, J., & Rennenberg, H. (2003). Emission of methane and nitrous oxide by Australian mangrove ecosystems. *Plant Biology*, *5*(4), 423–431. https://doi.org/10.1055/s-2003-42712

Kristensen, E. (2007). Carbon balance in mangrove sediments: The driving processes and their controls. Greenhouse gas and carbon balances in mangrove coastal ecosystems. *Gendai Tosho*, 61–78.

Lara, R. J., & Cohen, M. C. L. (2006). Sediment porewater salinity, inundation frequency and mangrove vegetation height in Braganca, North Brazil: An ecohydrology-based empirical model. *Wetlands Ecology and Management*, *14*(4), 349–358. https://doi.org/10.1007/s11273-005-4991-4

Le Quéré, C., Andrew, R. M., Friedlingstein, P., Sitch, S. (2018). Global carbon budget 2017. *Earth System Science Data*, *10*(1), 405–448.

Lee, R. Y., Porubsky, W. P., Feller, I. C., McKee, K. L., & Joye, S. B. (2008). Porewater biogeochemistry and soil metabolism in dwarf red mangrove habitats (Twin Cays, Belize). *Biogeochemistry*, *87*(2), 181–198. https://doi.org/10.1007/s10533-008-9176-9

Leopold, A., Marchand, C., Renchon, A., Deborde, J., Quiniou, T., & Allenbach, M. (2016). Net ecosystem CO_2 exchange in the "Coeur de Voh" mangrove, New Caledonia: Effects of water stress on mangrove productivity in a semi-arid climate. *Agricultural and Forest Meteorology*, *223*, 217–232. https://doi.org/10.1016/j.agrformet.2016.04.006

Lewis, E., & Perkin, R. (1981). The practical salinity scale 1978: Conversion of existing data. Deep Sea Research Part A. *Oceanographic Research Papers*, *28*(4), 307–328. https://doi.org/10.1016/0198-0149(81)90002-9

Li, H., Dai, S., Ouyang, Z., Xie, X., Guo, H., Xiao, X., et al. (2018). Multi-scale temporal variation of methane flux and its controls in a subtropical tidal salt marsh in eastern China. *Biogeochemistry*, *137*(1–2), 163–179. https://doi.org/10.1007/s10533-017-0413-y

Lin, P. (2001). *The comprehensive report of science investigation on the natural reserve of mangrove wetland of Zhangjiang Estuary in Fujian*. Xiamen University Press.

Liu, J., & Lai, D. Y. (2019). Subtropical mangrove wetland is a stronger carbon dioxide sink in the dry than wet seasons. *Agricultural and Forest Meteorology*, *278*, 107644. https://doi.org/10.1016/j.agrformet.2019.107644

Liu, J., Zhou, Y., Valach, A., Shortt, R., Kasak, K., Rey-Sanchez, C., et al. (2020). Methane emissions reduce the radiative cooling effect of a subtropical estuarine mangrove wetland by half. *Global Change Biology*. https://doi.org/10.1111/gcb.15247

Lloyd, J., & Taylor, J. A. (1994). On the temperature dependence of soil respiration. *Functional Ecology*, *8*(3), 315–323. https://doi.org/10.2307/2389824

Maher, D. T., Sippo, J. Z., Tait, D. R., Holloway, C., & Santos, I. R. (2016). Pristine mangrove creek waters are a sink of nitrous oxide. *Scientific Reports*, *6*. https://doi.org/10.1038/srep25701

Mauder, M., Cuntz, M., Drüe, C., Graf, A., Rebmann, C., Schmid, H. P., et al. (2013). A strategy for quality and uncertainty assessment of long-term eddy-covariance measurements. *Agricultural and Forest Meteorology*, *169*, 122–135. https://doi.org/10.1016/j.agrformet.2012.09.006

McLeod, E., Chmura, G. L., Bouillon, S., Salm, R., Björk, M., Duarte, C. M., et al. (2011). A blueprint for blue carbon: Toward an improved understanding of the role of vegetated coastal habitats in sequestering CO_2. *Frontiers in Ecology and the Environment*, *9*(10), 552–560. https://doi.org/10.1890/110004

Michaelis, L., & Menten, M. L. (1913). The kinetics of the inversion effect. *Biochemische Zeitschrift*, *49*, 333–369.

Moffat, A. M., Papale, D., Reichstein, M., Hollinger, D. Y., Richardson, A. D., Barr, A. G., et al. (2007). Comprehensive comparison of gap-filling techniques for eddy covariance net carbon fluxes. *Agricultural and Forest Meteorology*, *147*(3–4), 209–232. https://doi.org/10.1016/j.agrformet.2007.08.011

Murdiyarso, D., Hergoualc'h, K., & Verchot, L. V. (2010). Opportunities for reducing greenhouse gas emissions in tropical peatlands. *Proceedings of the National Academy of Sciences*, *107*(46), 19655–19660. https://doi.org/10.1073/pnas.0911966107

Nellemann, C., & Corcoran, E. (2009). *Blue carbon: The role of healthy oceans in binding carbon: A rapid response assessment*. UNEP/Earthprint.

Neubauer, S. C. (2014). On the challenges of modeling the net radiative forcing of wetlands: Reconsidering Mitsch et al. *Landscape Ecology*, *29*(4), 571–577. https://doi.org/10.1007/s10980-014-9986-1.2013

Neubauer, S. C., & Megonigal, J. P. (2015). Moving beyond global warming potentials to quantify the climatic role of ecosystems. *Ecosystems*, *18*(6), 1000–1013. https://doi.org/10.1007/s10021-015-9879-4

Ouyang, X., & Lee, S. Y. (2020). Improved estimates on global carbon stock and carbon pools in tidal wetlands. *Nature Communications*, *11*(1), 1–7. https://doi.org/10.1038/s41467-019-14120-2

Philipp, K., Juang, J.-Y., Deventer, M. J., & Klemm, O. (2017). Methane emissions from a subtropical grass marshland, northern Taiwan. *Wetlands*, *37*(6), 1145–1157. https://doi.org/10.1007/s13157-017-0947-8

Poffenbarger, H. J., Needelman, B. A., & Megonigal, J. P. (2011). Salinity influence on methane emissions from tidal marshes. *Wetlands*, *31*(5), 831–842. https://doi.org/10.1007/s13157-011-0197-0

Reichstein, M., Falge, E., Baldocchi, D., Papale, D., Aubinet, M., Berbigier, P., et al. (2005). On the separation of net ecosystem exchange into assimilation and ecosystem respiration: Review and improved algorithm. *Global Change Biology*, *11*(9), 1424–1439. https://doi.org/10.1111/j.1365-2486.2005.001002.x

Rinne, J., Tuittila, E.-S., Peltola, O., Li, X., Raivonen, M., Alekseychik, P., et al. (2018). Temporal variation of ecosystem scale methane emission from a boreal fen in relation to temperature, water table position, and carbon dioxide fluxes. *Global Biogeochemical Cycles*, *32*(7), 1087–1106. https://doi.org/10.1029/2017gb005747

Robertson, A. I., & Alongi, D. M. (2016). Massive turnover rates of fine root detrital carbon in tropical Australian mangroves. *Oecologia*, *180*(3), 841–851. https://doi.org/10.1007/s00442-015-3506-0

Rodda, S. R., Thumaty, K. C., Jha, C. S., & Dadhwal, V. K. (2016). Seasonal variations of carbon dioxide, water vapor and energy fluxes in tropical Indian mangroves. *Forests*, *7*(2). https://doi.org/10.3390/f7020035

Rosentreter, J. A., Maher, D. T., Erler, D. V., Murray, R., & Eyre, B. D. (2018a). Seasonal and temporal CO_2 dynamics in three tropical mangrove creeks - A revision of global mangrove CO_2 emissions. *Geochimica et Cosmochimica Acta*, *222*, 729–745. https://doi.org/10.1016/j.gca.2017.11.026

Rosentreter, J. A., Maher, D. T., Erler, D. V., Murray, R. H., & Eyre, B. D. (2018b). Methane emissions partially offset "blue carbon" burial in mangroves. *Science advances*, *4*(6), eaao4985. https://doi.org/10.1126/sciadv.aao4985

Sasmito, S. D., Taillardat, P., Clendenning, J. N., Friess, D. A., Murdiyarso, D., & Hutley, L. B., (2019). Effect of land-use and land-cover change on mangrove blue carbon: A systematic review. *Global Change Biology*, *0*(0).

Sturtevant, C., Ruddell, B. L., Knox, S. H., Verfaillie, J., Matthes, J. H., Oikawa, P. Y., & Baldocchi, D. (2016). Identifying scale-emergent, nonlinear, asynchronous processes of wetland methane exchange. *Journal of Geophysical Research: Biogeosciences*, *121*(1), 188–204. https://doi.org/10.1002/2015jg003054

Takemura, T., Hanagata, N., Sugihara, K., Baba, S., Karube, I., & Dubinsky, Z. (2000). Physiological and biochemical responses to salt stress in the mangrove, Bruguiera gymnorrhiza. *Aquatic Botany*, *68*(1), 15–28. https://doi.org/10.1016/s0304-3770(00)00106-6

Tang, A. C., Stoy, P. C., Hirata, R., Musin, K. K., Aeries, E. B., Wenceslaus, J., & Melling, L. (2018). Eddy covariance measurements of methane flux at a tropical peat forest in Sarawak, Malaysian Borneo. *Geophysical Research Letters*, *45*(9), 4390–4399. https://doi.org/10.1029/2017gl076457

Timmers, P. H., Welte, C. U., Koehorst, J. J., Plugge, C. M., Jetten, M. S. M., & Stams, A. J. M. (2017).*Reverse methanogenesis and respiration in methanotrophic archaea*.

Welti, N., Hayes, M., & Lockington, D. (2017). Seasonal nitrous oxide and methane emissions across a subtropical estuarine salinity gradient. *Biogeochemistry*, *132*(1–2), 55–69. https://doi.org/10.1007/s10533-016-0287-4

Whiting, G., & Chanton, J. (1993). Primary production control of methane emission from wetlands. *Nature*, *364*(6440), 794–795. https://doi.org/10.1038/364794a0

Xu, D.-Q., & Shen, Y.-K. (1996). *Handbook of photosynthesis* (pp. 451–459). Midday depression of photosynthesis.

Zheng, X., Guo, J., Song, W., Feng, J., & Lin, G. (2018). Methane emission from mangrove wetland soils is marginal but can be stimulated significantly by anthropogenic activities. *Forests*, *9*(12), 738. https://doi.org/10.3390/f9120738

Zhu, X., Hou, Y., Weng, Q., & Chen, L. (2019a). Integrating UAV optical imagery and LiDAR data for assessing the spatial relationship between mangrove and inundation across a subtropical estuarine wetland. *ISPRS Journal of Photogrammetry and Remote Sensing*, *149*, 146–156. https://doi.org/10.1016/j.isprsjprs.2019.01.021

Zhu, X., Hou, Y., Zhang, Y., Lu, X., Liu, Z., & Weng, Q. (2021a). Potential of sun-induced chlorophyll fluorescence for indicating mangrove canopy photosynthesis. *Journal of Geophysical Research: Biogeosciences*, *126*, e2020JG006159. https://doi.org/10.1029/2020jg006159

Zhu, X., Qin, Z., & Song, L. (2021b). How land-sea interaction of tidal and sea breeze activity affect mangrove net ecosystem exchange? *Journal of Geophysical Research: Atmosphere*, *126*, e2020JD034047. https://doi.org/10.1029/2020jd034047

Zhu, X., Song, L., Weng, Q., & Huang, G. (2019b). Linking in situ photochemical reflectance index measurements with mangrove carbon dynamics in a subtropical coastal wetland. *Journal of Geophysical Research: Biogeosciences*, *124*(6), 1714–1730. https://doi.org/10.1029/2019jg005022